Atmospheric Research 93 (2009) 874–887

Contents lists available at ScienceDirect

Atmospheric Research

journal homepage: www.elsevier.com/locate/atmos

Aerosol light absorption, black carbon, and elemental carbon at the Fresno Supersite, California

Judith C. Chow [a,b,*], John G. Watson [a,b], Prakash Doraiswamy [a,c], Lung-Wen Antony Chen [a], David A. Sodeman [a], Douglas H. Lowenthal [a], Kihong Park [a,d], W. Patrick Arnott [e], Nehzat Motallebi [f]

[a] Desert Research Institute, 2215 Raggio Parkway, Reno, NV, 89512, USA
[b] Institute of Earth Environment, Chinese Academy of Sciences, No. 10, Fenghui South Road, High-tech Zone, PO Box 17, Xian 710075, China
[c] Atmospheric Sciences Research Center at the University at Albany, State University of New York, Albany, NY, USA
[d] Gwangju Institute of Science and Technology, Dept. of Environmental Science and Engineering, 1 Oryong-dong, Buk-gu, Gwangju, 500-712, Republic of Korea
[e] University of Nevada, Department of Physics, 1664 N. Virginia Street, Reno, NV, 89557, USA
[f] California Air Resources Board, 1001 "I" Street, Sacramento, CA, 95812, USA

ARTICLE INFO

Article history:
Received 15 July 2008
Received in revised form 6 April 2009
Accepted 19 April 2009

Keywords:
Light absorption
Black carbon
Supersite
Organic carbon
Elemental carbon

ABSTRACT

Particle light absorption (b_{ap}), black carbon (BC), and elemental carbon (EC) measurements at the Fresno Supersite during the summer of 2005 were compared to examine the equivalency of current techniques, evaluate filter-based b_{ap} correction methods, and determine the EC mass absorption efficiency (σ_{ap}) and the spectral dependence of b_{ap}. The photoacoustic analyzer (PA) was used as a benchmark for in-situ b_{ap}. Most b_{ap} measurement techniques were well correlated ($r \geq 0.95$). Unadjusted Aethalometer (AE) and Particle Soot Absorption Photometer (PSAP) b_{ap} were up to seven times higher than PA b_{ap} at similar wavelengths because of absorption enhancement by backscattering and multiple scattering. Applying published algorithms to correct for these effects reduced the differences to 24 and 17% for the AE and PSAP, respectively, at 532 nm. The Multi-Angle Absorption Photometer (MAAP), which accounts for backscattering effects, overestimated b_{ap} relative to the PA by 51%. BC concentrations determined by the AE, MAAP, and Sunset Laboratory semi-continuous carbon analyzer were also highly correlated ($r \geq 0.93$) but differed by up to 57%. EC measured with the IMPROVE/STN thermal/optical protocols, and the French two-step thermal protocol agreed to within 29%. Absorption efficiencies determined from PA b_{ap} and EC measured with different analytical protocols averaged 7.9 ± 1.5, 5.4 ± 1.1, and 2.8 ± 0.6 m^2/g at 532, 670, and 1047 nm, respectively. The Angström exponent (α) determined from adjusted AE and PA b_{ap} ranged from 1.19 to 1.46. The largest values of α occurred during the afternoon hours when the organic fraction of total carbon was highest. Significant biases associated with filter-based measurements of b_{ap}, BC, and EC are method-specific. Correcting for these biases must take into account differences in aerosol concentration, composition, and sources.

1. Introduction

Aerosol light absorption reduces visibility (Chow et al., 2002; Watson, 2002), affects the earth's radiation balance (McCracken, 2008), and indicates the presence of combustion particles that adversely affect public health (Chow et al., 2006a; Pope and Dockery, 2006; Mauderly and Chow, 2008). Light absorbing particles radiate long-wave energy that heats the surrounding air. This results in a positive (warm) forcing which exceeds that of methane (the third most important greenhouse gas after carbon dioxide and water vapor) on a global scale (Jacobson, 2001). Light absorbing aerosols may

* Corresponding author. Desert Research Institute, 2215 Raggio Parkway, Reno, NV, 89512, USA. Tel.: +1 775 674 7050; fax: +1 775 674 7009.
E-mail address: judith.chow@dri.edu (J.C. Chow).

0169-8095/$ – see front matter © 2009 Elsevier B.V. All rights reserved.
doi:10.1016/j.atmosres.2009.04.010

produce a larger indirect positive forcing by enhancing cloud evaporation in the tropics (Ackerman et al., 2000).

Characterizing light absorbing aerosol is conceptually ambiguous (Watson et al., 2004, 2005). "Black carbon" (BC), or "soot," is an optical term that is commonly used to denote highly light-absorbing carbon. In most environments, BC produced by incomplete combustion of fossil- and bio-fuels dominates particle light absorption (b_{ap}; Horvath, 1993). "Elemental carbon" (EC) is a chemical term that refers to thermally-refractory pure carbon with a graphitic structure. However, neither pure carbon nor graphite is commonly observed in the atmosphere. BC may contain not only EC but organic carbon (OC) that efficiently absorbs light at blue and near-ultraviolet (UV) wavelengths (Andreae and Gelencser, 2006).

The most common approach for measuring b_{ap} involves collecting particles on a filter and measuring the reduction of light transmitted through the filter. Continuous instruments based on this principle include the Aethalometer (AE; Magee Scientific Co., Berkeley, CA), the Particle Soot Absorption Photometer (PSAP; Radiance Research, Seattle, WA), and the Multi-Angle Absorption Photometer (MAAP; Thermo Scientific, Waltham, MA). These filter-based methods experience three potential artifacts: 1) back-scattered light from particles in the filter; 2) enhancement of multiple scattering by highly-diffusive filter material and by particles on or embedded in the filter; and 3) reduction of multiple scattering by increased particle loading and b_{ap}. Both the AE and PSAP measure absorption when presented with non-absorbing aerosol particles (Bond et al., 1999; Arnott et al., 2005). Appropriate corrections must be applied to yield accurate b_{ap}. Recent developments allow for the direct measurement of b_{ap} in-situ under ambient conditions. The photoacoustic analyzer (PA) is a measure of b_{ap} derived from first principles (Bell, 1881) that detects the acoustic signal produced when the sample stream is heated via the absorption of laser light by particles in the air (Japar et al., 1982; Roessler, 1984; Arnott et al., 1999). With appropriate calibration and baseline correction for absorption by gases (Arnott et al., 2000), PA is a fundamental standard for b_{ap}.

Thermal/optical and thermal techniques have been used to measure carbon that evolves from an aerosol filter sample for various temperatures and carrier gases (Cachier et al., 1989a,b; Chow et al., 1993, 2007a; Birch and Cary, 1996a,b; Schmid et al., 2001; Currie et al., 2002; Watson et al., 2005). The more refractory carbon fraction is designated as EC, although the distinction between OC and EC is operationally defined. Inter-comparisons have shown that EC concentrations measured with different thermal/optical protocols differ by up to an order of magnitude (Birch, 1998; Chow et al., 2001, 2004; Schmidt et al., 2001; Currie et al., 2002; Watson et al., 2005; Park et al., 2006). The uncertainties of b_{ap} and EC measurements may contribute to the wide range (2–25 m^2/g) of reported mass absorption efficiencies (σ_{ap}; Bond and Bergstrom, 2006), i.e., absorption per unit mass concentration. These uncertainties complicate attempts to estimate aerosol radiative forcing in climate models.

BC concentration ($\mu g/m^3$) cannot be measured directly but must be inferred from b_{ap}. The link between b_{ap} and BC is σ_{ap}. Both b_{ap} and σ_{ap} depend on the incident wavelength (λ) and particle size, density, refractive index, chemical mixing state, and morphology (Bond, 2001; Bond and Bergstrom, 2006; Chen et al., 2006). There are no standards for BC or EC that can be used to reconcile various measurement techniques (Watson et al., 2005; Bond and Bergstrom, 2006).

Common goals of the Fresno Supersite (Watson et al., 2000) and California Black Carbon Characterization (Chow et al., 2006b, 2009) programs were to: 1) compare techniques for measuring b_{ap}, BC, and EC; and 2) determine the uncertainties in these measurements. The Reno Aerosol Optics Study (RAOS) made similar comparisons using laboratory-generated aerosols composed of mixtures of kerosene soot and ammonium sulfate [$(NH_4)_2SO_4$; Sheridan et al., 2005]. Algorithms were developed for correcting b_{ap} for the artifacts described above, but these have not been extensively tested for complex ambient aerosols. Park et al. (2006) compared b_{ap}, BC, and EC measurements at Fresno from December 2003 to November 2004. They examined the spectral dependence of b_{ap}, described by the Angström Power Law:

$$b_{ap} = k\,\lambda^{-\alpha}, \quad (1)$$

where α is the Angström exponent (approximately 1 for kerosene soot; Sheridan et al., 2005), k is a constant and λ is the wavelength in units of length. The objectives of this study are to: 1) expand the work by Park et al. (2006) to include additional measurement techniques; 2) evaluate the effectiveness of the application of RAOS b_{ap} correction algorithms to Fresno aerosols; and 3) determine the variation of σ_{ap} and α at Fresno during the summer of 2005.

2. Methods

Measurements were made at the Fresno Supersite at 3425 First Street in Fresno, CA (119.7727725 °W and 36.78184232 °N), located approximately 5.5 km north-northeast of the downtown district and surrounded by commercial buildings, schools, and residences. First Street is a four-lane artery with moderate traffic levels. Fresno, located in California's San Joaquin Valley (SJV), is influenced by emissions from various sources including diesel and gasoline vehicles, cooking, residential wood combustion, and agricultural activities; relative source contributions vary diurnally and seasonally (Magliano et al., 1999; Schauer and Cass, 2000; Chen et al., 2007; Chow et al., 2007b; Watson et al., 2008). Elevated ozone (O_3) concentrations and high secondary organic aerosol (SOA) production from gaseous precursors are expected during summer (e.g., Watson et al., 2006).

Continuous and time-integrated particle and gas monitors were operated at the Fresno Supersite from May 1999 through February 2007 (Watson et al., 2000; Chow et al., 2008). Table 1 documents the carbon measurements during an intensive experiment conducted from August 1 to September 30, 2005. Measurements included in-situ continuous BC or b_{ap} (i.e., two wavelength and seven-color AE [2-AE, 7-AE], PSAP, MAAP, PA), and hourly EC (Carbon Aerosol Analysis Field Instrument; Sunset Laboratory, Tigard, OR; Bae et al., 2004), continuous particle light scattering (b_{sp}; three wavelength nephelometer; Model 3563, TSI, Inc., Shoreview, MN), and 24-hour integrated $PM_{2.5}$ mass and chemical measurements (i.e., Federal Reference Method [FRM], Reference Ambient Air Sampler [RAAS], and $PM_{2.5}$ high-volume [HiVol] samplers). The continuous monitors

Table 1
Thermal and optical measurements at the Fresno Supersite, CA, between August 1, 2005 and September 30, 2005.

Observable (unit) [a]	Wavelength (nm)	Instrument	Abbreviation	Model	Manufacturer	Measurement principle [b]	Inlet [c]	Collection medium	Flow rate (L/min)	Averaging time
b_{ap} (Mm^{-1}); BC ($\mu g/m^3$)	370, 880	Dual-wavelength aethalometer	2-AE	AE-21	Magee Scientific, Inc., Berkeley, CA	Light transmission through the quartz-fiber filter tape is continuously monitored and the light attenuation is converted to BC using σ^*_{ap} of 14,625/λ (m^2/g), where λ is in nm. Reports BC concentration at 20 °C and 1013.25 mb (Hansen et al., 1984).	$PM_{2.5}$ cyclone	Quartz-fiber filter tape	6.6	5 min
b_{ap} (Mm^{-1}); BC ($\mu g/m^3$)	370, 470, 520, 590, 660, 880, 950	Seven-color aethalometer	7-AE	AE-31	Magee Scientific, Inc., Berkeley, CA		$PM_{2.5}$ cyclone	Quartz-fiber filter tape	6.7	5 min
b_{ap} (Mm^{-1})	467, 530, 660	Three wavelength particle soot absorption photometer	PSAP	Three wavelength model	Radiance Research, Seattle, WA	Light transmission through the glass-fiber filter is continuously monitored to estimate b_{ap}. Includes an empirical factor that accounts for scattering by the filter matrix and for the non-linear instrument response as a function of loading. Reports b_{ap} at 0 °C and 1013.25 mb.	$PM_{2.5}$ cyclone	Glass-fiber filter	0.5	3 s
b_{ap} (Mm^{-1}); BC ($\mu g/m^3$)	670	Multi-angle absorption photometer	MAAP	5012	Thermo Scientific, Franklin, MA	Light transmission through the glass-fiber filter tape is continuously monitored at 0° and reflectance is monitored at 130° and 165° from the projected light beam. A two-stream-approximation radiative transfer model calculates b_{ap}. A σ^*_{ap} of 6.6 m^2/g converts b_{ap} to BC and is reported for ambient temperature and pressure (Petzold et al., 2002, 2005; Petzold and Schönlinner, 2004).	$PM_{2.5}$ cyclone	Glass-fiber filter tape	16.7	1 min
b_{ap} (Mm^{-1})	532 1047	Photoacoustic (two instruments at different wavelengths)	PA	n/a [c]	Desert Research Institute, Reno, NV	Particles are drawn into a cavity and illuminated by a laser with the desired wavelength modulated at the resonant frequency of the cavity. The heating and cooling of the particle in response to the absorbed light creates a sound wave that is detected by a microphone. The intensity of the acoustic wave is related to b_{ap}. by calibration with NO_2 absorption (Arnott et al., 1999). Results are reported at ambient temperature and pressure.	$PM_{2.5}$ cyclone	In-situ: acoustic resonator	1 1	4 s 3 s

Thermal EC, OC and TC ($\mu g/m^3$)	660	Semi-continuous carbon aerosol analysis field instrument	Sunset	Semi-continuous field instrument	Sunset Laboratory, Tigard, OR	Particles collected on the quartz-fiber filter are subject to thermal/optical analysis following NIOSH 5040 TOT protocol. Evolved CO_2 is analyzed by NDIR. Laser transmittance is used to correct for pyrolysis.	$PM_{2.5}$ cyclone	Quartz-fiber filter tape	8.5	1 h
Optical BC ($\mu g/m^3$)	660					During the particle collection phase, light transmission through the filter is monitored to quantify BC similar to an aethalometer (Bae et al., 2004). Reports BC, EC, OC, and TC concentrations for ambient conditions.				
b_{sp} (Mm^{-1})	450, 550, 700	Three wavelength nephelometer	Neph	3563	TSI Inc., Shoreview, MN	A light source illuminates the sample air and the light scattered by particles at angles between 7° and 170° is detected. The b_{sp} is reported at ambient temperature and pressure. Zero air calibrations are performed using particle-free air every hour.	$PM_{2.5}$ cyclone	None. Analysis is done in-situ	20	5 min
EC, OC, and TC ($\mu g/m^3$); b_{ap} (Mm^{-1})	632.8	FRM filter samples analyzed following the IMPROVE_A_TOR and IMPROVE_A_TOT protocols	FRM	Andersen 100	Thermo Scientific, Franklin, MA	Particles collected on a quartz-fiber filter at ambient temperature and pressure are subject to different temperature ramps at ambient temperature and pressure following the IMPROVE_A protocol (Chow et al., 1993, 2001, 2004, 2005a, 2007a). The evolved carbon is converted to CH_4 and analyzed by FID. Pyrolysis correction using laser reflectance is termed TOR, and that based on laser transmittance is termed TOT.	WINS impactor	EC, OC, and TC from quartz-fiber; b_{ap} from Teflon-membrane filters	16.7	24 h
EC, OC, and TC ($\mu g/m^3$); b_{ap} (Mm^{-1})	632.8	RAAS filter samples analyzed following the IMPROVE_A_TOR, IMPROVE_A_TOT, STN_TOR, and STN_TOT protocols	RAAS	Andersen RAAS 400	Thermo Scientific, Franklin, MA	Particles collected on a quartz-fiber filter at ambient temperature and pressure are subject to thermal carbon analysis following the IMPROVE_A (Chow et al., 1993, 2001, 2004, 2005a, 2007a) and STN (Peterson and Richards, 2002) protocols. Pyrolysis corrections are made using laser reflectance (TOR) and laser transmittance (TOT).	$PM_{2.5}$ cyclone	EC, OC, and TC from quartz-fiber filters; b_{ap} from Teflon-membrane filters	16.7 (Channel I: undenuded Teflon); 7.3 (Channel II: undenuded Quartz)	24 h
EC, OC, and TC ($\mu g/m^3$)	632.8	High-volume sampler filters analyzed following the IMPROVE_A_TOR, IMPROVE_A_TOT, STN_TOR, STN_TOT, and French two-step protocols	HiVol	Sierra High-Volume sampler	Thermo Scientific, Franklin, MA	Particles collected on a quartz-fiber filter are subject to thermal carbon analysis following the IMPROVE_A (Chow et al., 1993, 2001, 2004, 2005a, 2007a), STN (Peterson and Richards, 2002), and French two-step (Cachier et al., 1989a,b) protocols.	Multiple $PM_{2.5}$ impactors	OC, EC, and TC from quartz-fiber filters	1130	24 h

[a] BC: Black carbon; OC: Organic carbon; EC: Elemental carbon; TC: Total carbon; b_{ap}: Light absorption.

[b] σ^*_{ap}: mass absorption efficiency; λ: wavelength; mb: millibar; NIOSH 5040 TOT: National Institute for Occupational Safety and Health (NIOSH) thermal/optical transmittance (TOT) 5040 protocol; CH_4: Methane; NDIR: Non-dispersive infrared detector; FID: Flame ionization detector; IMPROVE_A: Interagency Monitoring of PROtected Visual Environments protocol (Chow et al., 1993, 2007a) with pyrolysis correction using laser reflectance (TOR) and laser transmittance (TOT); STN: Speciation Trends Network protocol (Peterson and Richards, 2002) with pyrolysis correction using laser reflectance (TOR) and laser transmittance (TOT); French: Cachier et al. (1989a,b) French two-step protocol; see Table 2 for further details on different carbon analyses protocols using the DRI Model 2001 thermal/optical carbon analyzer (Desert Research Institute, Reno, NV).

[c] $PM_{2.5}$ cyclones are BGI sharp-cut cyclones (BGI, Waltham, MA) except for the photoacoustic instruments and the three wavelength nephelometer which were a Bendix 240 cyclone (now Tisch Environmental, Cleves, OH).

were operated in air-conditioned second-story rooms through manifolds preceded by $PM_{2.5}$ inlets ~10 m above the ground.

Quartz-fiber filters from the FRM, RAAS and HiVol samplers were analyzed for OC and EC by three carbon protocols (Table 2) commonly used in the U.S. and Europe: 1) Interagency Monitoring of PROtected Visual Environments (IMPROVE_A) thermal/optical reflectance and transmittance protocol (IMPROVE_A_TOR and IMPROVE_A_TOT, respectively; Chow et al., 1993, 2001, 2004, 2005a, 2007a), 2) the Speciation Trends Network (STN) TOR and TOT (STN_TOR and STN_TOT, respectively; Peterson and Richards, 2002); and 3) the French two-step thermal method (Cachier et al., 1989a,b).

PA b_{ap} measured at 532 nm and 1047 nm was adjusted for absorption by nitrogen dioxide (NO_2) by alternating the sample flow with HEPA (High-Efficiency Particulate Air)-filtered air for five minutes out of every hour (Arnott et al., 2000). The 7-AE and the PSAP b_{ap} were adjusted for multiple scattering, filter loading, and back-scattering effects using b_{sp} measurements from the TSI three wavelength nephelometer following procedures described by Arnott et al. (2005) and Virkkula et al. (2005), respectively. The MAAP compensates for multiple- and back-scattering effects using a radiative transfer model based on simultaneous reflectance and transmittance measurements (Petzold et al., 2002).

Refining the AE b_{ap} values (Arnott et al., 2005) involves: 1) using b_{sp} measurements from the collocated nephelometer; 2) estimating b_{sp} at the wavelengths of the 7-AE; and 3) adjusting for truncation errors (Anderson and Ogren, 1998) inherent in the nephelometer measurements. Adjustments for 7-AE b_{ap} were estimated from Table 1 of Arnott et al. (2005). These values were based on experiments with kerosene soot and pure $(NH_4)_2SO_4$ aerosols, but they did not provide good agreement between adjusted AE and PA b_{ap} for ambient aerosols in Las Vegas, NV (Arnott et al., 2005). To reconcile those differences, Arnott et al. (2005) substituted values of 3.688 and 0.2338 for M (multiple scattering correction term) and $\tau_{a,f\chi}$ (transmission correction term), respectively, at 521 nm (Table 1 of Arnott et al., 2005). These values were used in this study and scaled to different AE wavelengths using the spectral dependence of Arnott et al. (2005). The AE tape was advanced when the attenuation [$ATN = -\ln(I/I_o)$; I/I_o = transmittance] reached 1. This value is within the range recommended by the manufacturer.

Adjustments for PSAP b_{ap} are similar to those for the AE. The PSAP internal transmission (τ) correction function [$f(\tau)^{-1}$] was set to ($1.237\,\tau + 0.814$). The uncorrected PSAP b_{ap} [PSAP (raw)] was obtained by multiplying the PSAP's b_{ap} output by $f(\tau)^{-1}$. PSAP(raw) was then adjusted for transmission and scattering effects using b_{sp} measured with the three wavelength nephelometer using the iterative procedure (Eqs. (7)–(9) and Table 3) of Virkkula et al. (2005). Nephelometer b_{sp} was interpolated to the wavelength of the PSAP and adjusted for truncation errors prior to being used to adjust b_{ap}. The PSAP was attended regularly and the filter was changed when the transmittance reached 0.7. Five-minute average PSAP data were voided if the transmittance was less than 0.5. The original

Table 2
Thermal/optical and thermal carbon analysis protocols applied in this study.

	Carbon fraction	IMPROVE_A_TOR/TOT [a]			STN_TOR/TOT [b]			Modified French two-step [c]		
		Carrier gas	Temperature (°C)	Residence time (s)	Carrier gas	Temperature (°C)	Residence time (s)	Carrier gas	Temperature (°C)	Residence time (s)
OC	OC1	He	140	150 to 580 [d]	He	310	60	O_2	340	7200
	OC2	He	280	150 to 580	He	480	60			
	OC3	He	480	150 to 580	He	615	60			
	OC4	He	580	150 to 580	He	900	90			
		He	–	–	He	Cool oven	–			
EC	EC1	O_2/He [e]	580	150 to 580	O_2/He [e]	600	45	EC was determined using the IMPROVE_A protocol by analyzing the remaining carbon content (i.e., the TC left) on the punch after the pre-combustion phase. Thus, TC from the IMPROVE_A analysis is used to calculate OC content by the French protocol.		
	EC2	O_2/He	740	150 to 580	O_2/He	675	45			
	EC3	O_2/He	840	150 to 580	O_2/He	750	45			
	EC4	O_2/He	N/A	N/A	O_2/He	825	45			
	EC5	O_2/He	N/A	N/A	O_2/He	920	120			

[a] IMPROVE_A_TOR/TOT: thermal/optical carbon analysis following the IMPROVE_A (Interagency Monitoring of PROtected Visual Environments) protocol (Chow et al., 2007a) using the DRI Model 2001 thermal/optical carbon analyzer (Atmoslytic, Inc., Calabasas, CA). The evolved carbon is converted to carbon dioxide (CO_2) and reduced to methane (CH_4) which is detected using a flame ionization detector (FID). The correction for pyrolyzed organic carbon (OP) is done by monitoring the reflectance (TOR) or transmittance (TOT) using a 632.8 nm laser. OP is defined as the carbon that evolves between the introduction of O_2 and the return of reflectance (TOR) or transmittance (TOT) to its initial value. OC equals OC1 + OC2 + OC3 + OC4 + OP, and EC equals EC1 + EC2 + EC3 − OP. Total carbon (TC) equals OC + EC.

[b] STN_TOR/TOT: carbon analysis following the STN (Speciation Trends Network) protocol (Peterson and Richards, 2002)using the DRI Model 2001 analyzer. The standard STN protocol uses transmittance to correct for pyrolysis (TOT). In this study, reflectance was also recorded during the STN analyses, which is reported as STN_TOR (i.e., uses STN temperature protocols, with reflectance for pyrolysis correction).

[c] Modified French two-step: thermal carbon analysis following the two-step protocol reported by Cachier et al. (Cachier et al., 1989a,b), modified to enable analysis using the DRI Model 2001 analyzer. In the original protocol, OC is vaporized during the pre-combustion phase at 340 °C in 100% O_2 atmosphere, and EC is determined using coulometric titration of CO_2 and measuring the remaining carbon content on the filter by combustion at 1100 °C in 100% O_2,. TC is determined from another punch by coulometric titration. In this study, ~0.5 cm^2 punch was heated at 340 °C in 100% O_2 for 2 h (pre-combustion phase that is supposed to volatilize all OC), following which this punch was analyzed using the IMPROVE_A protocol to determine the remaining carbon content, which is taken to be the EC. TC was determined by analyzing another punch for the total carbon content directly with the IMPROVE_A protocol without subjecting it to the pre-combustion phase. OC is obtained by difference (OC = TC − EC). This protocol does not correct for charring.

[d] The residence time at each temperature in the IMPROVE_A protocol depends on when the FID signal returns to its baseline, to obtain well-defined carbon fraction peaks, with a minimum of 150 s and a maximum of 580 s at each temperature.

[e] 2% oxygen (O_2) and 98% helium (He) atmosphere.

Table 3
Instrument uncertainty and minimum detection limits (MDL).[a]

Instrument	Coefficient of Variation (CV in %)[b]	Minimum Detectable Limit (MDL)[c]	Reference
2-AE (370 and 880 nm), 7-AE (370, 470, 520, 590, 660, 880, and 950 nm)	10%, based on collocated measurements	5-min: 0.060 μg/m^3 [e] (370 nm: 2.37 Mm^{-1} 470 nm: 1.87 Mm^{-1} 520 nm: 1.69 Mm^{-1} 590 nm: 1.49 Mm^{-1} 660 nm: 1.33 Mm^{-1} 880 nm: 1.00 Mm^{-1} 950 nm: 0.92 Mm^{-1})	Hansen (2005)
PSAP (467, 530, and 660 nm)	8%	467 nm: 0.32 Mm^{-1} [c, f] 530 nm: 0.09 Mm^{-1} [c, f] 660 nm: 0.06 Mm^{-1} [c, f]	Virkkula et al. (2005)
MAAP (670 nm)	12%	2-min: 0.1 μg/m^3; 0.66 Mm^{-1} 1-min: 0.141 μg/m^3; 0.93 Mm^{-1}	Petzold et al. (2002)
PA (532 and 1047 nm)	5-min average instrument noise reported by the instrument was taken to be the measurement uncertainty	10 min: 0.4 Mm^{-1} [g]	Arnott et al. (1999)
Sunset (660 nm)	TC = 10% Thermal OC = 10% Thermal EC = 20% Optical BC = 10%	TC = 0.4 μg/m^3 OC = 0.2 μg/m^3 EC = 0.2 μg/m^3 BC = 0.09 Mm^{-1}	Bae et al. (2004)
TSI three-color nephelometer[d] (450, 550, and 700 nm)	5%	450 nm: 1.45 Mm^{-1} [h] 550 nm: 0.92 Mm^{-1} [h] 700 nm: 0.58 Mm^{-1} [h]	Anderson and Ogren (1998)

[a]The MDL was used to estimate the measurement uncertainty as $\sqrt{(CV \times c_i)^2 + MDL^2}$, where c_i is the measured value (b_{ap} or EC/OC/BC).
[b]CV is the coefficient of variation, defined as the standard deviation divided by the average.
[c]Interpolated from one time basis to another as follows:

$MDL_{t1} = MDL_{t2}\sqrt{\frac{t_2}{t_1}}$, where $t1$ and $t2$ are the two time bases.

[d]Used to estimate uncertainty for 7-AE (adj) and PSAP(adj) b_{ap} measurements by error propagation (Watson et al., 2001).
[e]Two times the upper limit of the standard deviation of 5-min BC measurements of particle-free air deemed acceptable by the manufacturer. Assumed to be the same at all wavelengths (λ). Equivalent MDL in terms of b_{ap} at each λ can be calculated using (0.06 × 14625/λ).
[f]Two times the standard deviation of 1-min noise (with 60 s cycle time) reported in Virkkula et al. (2005), converted to a 5-min basis.
[g]Assumed to be the same at both wavelengths (λ = 532 and 1047 nm).
[h]Two times the standard deviation of 5-min b_{sp} measurements between 08/01/2005 and 09/20/2005, recorded during the hourly auto-zero cycles in the nephelometer.

[uncorrected] b_{ap} are referred to as 2-AE (raw), 7-AE (raw) and PSAP(raw), while the adjusted values are denoted as 7-AE (adj) and PSAP(adj). The 2-AE (raw) measurements were not adjusted because they include data at only two wavelengths. BC and EC concentrations are standardized to 25 °C and 1013.25 millibar (mb) to facilitate comparisons.

The instrument-specific factors that translate b_{ap} to BC are analogous, but not necessarily equivalent, to σ_{ap} because of the measurement artifacts in different environments. The AE factor (14,625/λ) was derived from an experiment that compared measured b_{ap} with EC determined by the Lawrence Berkeley Laboratory (LBL) thermal analysis method (Gundel et al., 1984). The MAAP b_{ap} was converted to BC at 670 nm using 6.6 m^2/g based on experiments by Petzold et al. (2002) and Petzold and Schönlinner (2004). The Sunset Carbon Analyzer reports optical BC (in addition to thermal/optical EC) as BC = 0.75 b_{ap} + 2.25 b_{ap} (personal communication with Bob Cary at Sunset Laboratory).

Measurement precision can be described by the coefficient of variation (CV) and the minimum detectable limit (MDL). The CV and MDL are determined from replicate sample and blank measurements, respectively (Watson et al., 2001). CVs and MDLs for continuous measurements of b_{ap} and b_{sp} are shown in Table 3. Measurement uncertainties (σ) at the Fresno Supersite were calculated as follows:

$$\sigma_i = \sqrt{(CV \times c_i)^2 + MDL^2} \quad (2)$$

where c_i represents the ith individual measurement. The uncertainty of an average value is the square root of the sum of the squared individual uncertainties (root mean squared error [RMSE]).

3. Measurement comparisons

Watson and Chow (2002a) and Chow et al. (2005b) describe a combination of statistical measures for comparing collocated samplers with measurements y and x, which are utilized in the analyses presented here. These indices include: 1) the average values of y and x; 2) the slope, intercept, and standard errors of ordinary least squares (OLS) regressions of y on x (Bevington, 1969); 3) the correlation (r) between y and x; 4) the average and standard deviation of y/x; 5) the average of the paired differences ($y-x$), their standard deviation, the measurement uncertainty of the average of $y-x$ differences (RMSE), and the average error (AE), i.e., the average of $(y-x)/x$, expressed as a percent [average error = 100 $(y/x)-1$]; and 6) the distribution of $y-x$ with respect to their uncertainties, i.e., the percent of cases where $(y-x)$ is $<1\sigma_{y-x}$, $1\sigma_{y-x}<(y-x)<2\sigma_{y-x}$, $2\sigma_{y-x}<(y-x)<3\sigma_{y-x}$, and $(y-x)>3\sigma_{y-x}$, where $\sigma_{y-x} = \sqrt{\sigma_x^2 + \sigma_y^2}$.

3.1. Comparison of light absorption (b_{ap}) measurements

Table 4 compares hourly b_{ap} measured among different instruments. Most comparisons are for measurements made at similar wavelengths. Raw and adjusted b_{ap}, scaled to the MAAP λ = 670 nm, are compared for the 7-AE and PSAP to demonstrate the magnitude of the adjustment for each instrument. Unadjusted MAAP and PA b_{ap}, also scaled to

Table 4
Comparison statistics for hourly optical carbon (b_{ap}) measurements at the Fresno Supersite, CA.

Instrument		Averages		OLS Regression[a]				r	N[c]	y/x		y-x			$(y$-$x)/x$	Distribution of $y-x$[g]			
Y	x	y	x	Slope	SE[b]	Intercept	SE[b]			Average	SD[d]	Average	SD[d]	RMSE[e]	AE[f]	<1σ[e]	1σ-2σ	2σ-3σ	>3σ
		(Mm^{-1})		(Mm^{-1})								(Mm^{-1})			(%)	(%)			
7-AE (raw) 370 nm	2-AE (raw) 370 nm	36.36	34.08	1.09	0.01	−0.93	0.34	0.96	1302	1.07	0.17	2.28	6.69	6.84	7	76.8	21.0	2.0	0.2
7-AE (raw) 880 nm	2-AE (raw) 880 nm	16.44	15.29	1.13	0.01	−0.90	0.10	0.98	1302	1.06	0.11	1.14	2.38	3.07	6	90.7	8.8	0.5	0.0
7-AE (raw) 370 nm	7-AE (adj) 370 nm	35.44	11.97	2.31	0.02	7.83	0.28	0.97	1135	3.32	0.74	23.47	13.40	5.08	232	0.0	0.3	4.2	95.5
7-AE (raw) 590 nm	7-AE (adj) 590 nm	23.07	6.41	2.80	0.02	5.09	0.15	0.98	1135	4.11	0.99	16.66	9.98	3.27	311	0.0	0.3	2.4	97.4
7-AE (raw) 880 nm	7-AE (adj) 880 nm	16.03	4.20	2.97	0.02	3.56	0.10	0.98	1133	4.41	1.16	11.84	7.20	2.25	341	0.0	0.0	1.5	98.5
PSAP(raw) 467 nm	PSAP(adj) 467 nm	23.22	8.10	2.51	0.02	2.87	0.20	0.96	1093	2.99	0.35	15.13	8.27	2.30	199	0.0	0.0	0.0	100.0
PSAP(raw) 530 nm	PSAP(adj) 530 nm	20.57	6.74	2.64	0.02	2.76	0.17	0.97	1110	3.19	0.37	13.83	7.67	2.00	219	0.0	0.0	0.0	100.0
PSAP(inst) 530 nm[h]	PSAP(adj) 530 nm	10.34	6.74	1.45	0.01	0.60	0.05	0.99	1107	1.57	0.10	3.61	2.09	1.17	57	0.0	0.3	7.1	92.6
PSAP(raw) 660 nm	PSAP(adj) 660 nm	16.84	5.45	2.56	0.02	2.92	0.15	0.96	1118	3.28	0.43	11.39	6.39	1.65	228	0.0	0.0	0.0	100.0
7-AE (raw) 470 nm	PSAP(raw) 467 nm	27.01	22.39	1.26	0.01	−1.28	0.27	0.97	987	1.20	0.16	4.62	5.34	4.25	20	51.9	36.7	10.3	1.1
7-AE (raw) 520 nm	PSAP(raw) 530 nm	25.69	19.85	1.37	0.01	−1.47	0.24	0.97	1003	1.29	0.16	5.84	5.69	3.95	29	29.2	49.8	18.3	2.7
7-AE (raw) 660 nm	PSAP(raw) 660 nm	20.79	16.18	1.37	0.01	−1.30	0.18	0.98	1008	1.28	0.15	4.61	4.51	3.21	28	29.4	51.6	17.4	1.7
7-AE (adj) 470 nm	PSAP(adj) 467 nm	7.58	7.74	1.15	0.01	−1.30	0.10	0.96	954	0.93	0.18	−0.16	1.83	1.29	−7	62.6	29.2	6.8	1.4
7-AE (adj) 520 nm	PSAP(adj) 530 nm	7.21	6.44	1.29	0.01	−1.08	0.09	0.96	968	1.07	0.21	0.77	1.98	1.14	7	62.1	27.7	7.0	3.2
7-AE (adj) 660 nm	PSAP(adj) 660 nm	5.49	5.16	1.18	0.01	−0.59	0.08	0.95	969	1.02	0.21	0.33	1.49	0.88	2	59.3	31.3	6.5	2.9
7-AE (raw) 660 nm	MAAP 670 nm	23.61	6.76	3.56	0.02	−0.47	0.16	0.99	822	3.52	0.38	16.85	12.08	3.50	252	0.0	0.4	8.2	91.5
7-AE (adj) 660 nm	MAAP 670 nm	6.34	6.51	1.19	0.01	−1.41	0.08	0.97	676	0.90	0.18	−0.17	1.47	1.57	−10	86.5	12.7	0.6	0.1
PSAP(raw) 660 nm	MAAP 670 nm	16.81	6.40	2.48	0.01	0.96	0.11	0.99	607	2.68	0.21	10.41	6.45	2.08	168	0.0	0.2	4.3	95.6
PSAP(adj) 660 nm	MAAP 670 nm	5.35	6.40	0.90	0.01	−0.40	0.07	0.97	607	0.81	0.10	−1.05	1.01	1.44	−19	72.5	26.7	0.8	0.0
7-AE (raw) 520 nm	PA 532 nm	25.04	5.06	6.41	0.06	−7.41	0.32	0.96	1021	4.68	1.06	19.98	13.84	3.93	368	0.4	4.7	11.3	83.6
7-AE (adj) 520 nm	PA 532 nm	6.96	5.03	2.18	0.02	−4.01	0.12	0.95	984	1.24	0.43	1.92	3.25	2.14	24	63.9	20.5	8.9	6.6
7-AE (raw) 950 nm	PA 1047 nm	14.12	1.91	8.24	0.06	−1.60	0.12	0.98	1027	7.16	1.21	12.22	8.16	2.17	616	0.0	1.9	6.3	91.7
7-AE (adj) 950 nm	PA 1047 nm	3.56	1.90	2.55	0.02	−1.30	0.05	0.96	987	1.69	0.51	1.66	1.83	1.08	69	46.8	25.8	15.1	12.3
PSAP(raw) 530 nm	PA 532 nm	20.09	5.22	4.48	0.05	−3.29	0.27	0.95	1041	3.69	0.84	14.87	9.22	2.63	269	1.3	5.5	11.0	82.2
PSAP(adj) 530 nm	PA 532 nm	6.54	5.22	1.62	0.02	−1.94	0.09	0.95	1041	1.17	0.31	1.31	1.97	1.97	17	68.9	22.5	7.0	1.6
7-AE (adj) 670 nm	PA 670 nm	5.21	3.59	2.21	0.02	−2.70	0.08	0.96	930	1.30	0.42	1.62	2.42	2.05	30	68.8	18.1	8.6	4.5
PSAP(raw) 670 nm	PA 670 nm	16.04	3.71	4.92	0.04	−2.23	0.18	0.96	1041	4.14	0.84	12.33	7.60	2.43	314	1.9	9.3	11.6	77.1
PSAP(adj) 670 nm	PA 670 nm	5.09	3.71	1.76	0.02	−1.43	0.07	0.96	1041	1.28	0.33	1.38	1.66	1.99	28	70.1	22.0	6.2	1.6
MAAP 670 nm	PA 670 nm	6.27	3.88	1.99	0.02	−1.46	0.08	0.98	578	1.51	0.33	2.39	2.20	2.38	51	56.6	31.1	11.2	1.0

[a]Ordinary least squares regression.
[b]Standard error.
[c]Number of data pairs.
[d]Standard deviation.
[e]Root mean squared errors (RMSE) = square root of sum of squares of the uncertainties for x and y.
[f]AE = Average error, 100 (average of $(y-x)/x$).
[g]Measurement difference of $(y-x)$ and distribution of measurement differences.
[h]In this case, PSAP(inst) represents the instrument correction: $b_{ap}\times(1.237\tau+0.814)^{-1}$.

670 nm, are compared with raw and adjusted 7-AE and PSAP b_{ap}. Instrument-specific α and k in Eq. (1) were estimated from the linear regression of log(b_{ap}) on log λ:

$$\log\left(b_{ap}\right) = -\alpha \log \lambda + \log k. \quad (3)$$

For b_{ap} at 670 nm:

$$b_{ap}(670\ \text{nm}) = b_{ap}\left(\lambda_f\right)\left(\frac{670}{\lambda_f}\right)^{-\alpha}, \quad (4)$$

where λ_f, the reference wavelength, was taken as 660 nm for 7-AE and PSAP, and 532 nm for PA.

All pair-wise correlations (r) for continuous b_{ap} measurements in Table 4 equaled or exceeded 0.95 and thus met the criteria for predictability described by Watson and Chow (2002a). The best comparisons (i.e., slope close to unity and absolute average error ≤7%) were found between the 2-AE (raw) and 7-AE (raw) at 370 and 880 nm, respectively. The differences ($y-x$) were less than their uncertainties (1σ) for 77 and 91% of data pairs at 370 and 880 nm, respectively. Raw 2-AE, and raw and adjusted 7-AE and PSAP b_{ap} decreased with increasing wavelength as did MAAP and PA b_{ap}. Adjustments to 7-AE b_{ap} (y/x) ranged from 3.32 (370 nm) to 4.41 (880 nm).

Hourly nephelometer b_{sp} at 532 nm averaged $31 \pm 21\ \text{Mm}^{-1}$ and ranged from 4 to 150 Mm^{-1}. There was a moderate correlation ($r=0.66$) between b_{sp} and PA b_{ap} at 532 nm. Adjustments to PSAP b_{ap} ranged from factors of 2.99 (467 nm) to 3.28 (660 nm). The PSAP correction (PSAPCorr, the percent difference between raw and adjusted PSAP b_{ap} with respect to raw PSAP b_{ap}) was essentially linear. On an hourly basis, the correlation between PSAP(raw) and PSAP(adj) at 530 nm was 0.97 (Table 4). Virkkula et al. (2005) noted that PSAPCorr depends on the single-scattering albedo ($\omega = b_{sp}/[b_{sp}+b_{ap}]$). The hourly average ω, based on b_{sp} and PA b_{ap} at 532 nm, was 0.83 ± 0.06. Because the CV of ω was low (7%), the correlation between ω and PSAPCorr at 530 nm was moderate ($r=0.48$). However, the correlation between ω and PSAPCorr based on PSAP(adj) b_{ap} was higher (0.78) because the correction algorithm iteratively uses PSAP b_{ap} to calculate ω. Table 4 also compares PSAP(adj) b_{ap} with PSAP(inst) b_{ap} at 530 nm. In this case, PSAP(inst) results from the internal transmission correction: PSAP(raw) × $(1.237\,\tau + 0.814)^{-1}$.

Arnott et al. (2003) and Murphy (2009) examine the effects of relative humidity (RH) on both PA and PSAP b_{ap} measurements, demonstrating that the photoacoustic signal in the PA is reduced at RH >70%. The PSAP displayed an erratic response with increasing RH which was explained in part by absorption of hydrated aerosol solution by the PSAP cellulose-membrane filter backing. The hourly average ambient RH during the summer experiment in Fresno was low (46 ± 19%). However, the continuous instruments were located indoors in air-conditioned rooms. The only measurement of sample air RH was in the TSI three wavelength nephelometer, where the hourly average RH was 33 ± 6%. Fig. 1 shows relationships among hourly average ambient RH (RH_{amb}), RH in the nephelometer (RH_{TSI}), ω based on PA b_{ap} at 532 nm and PSAP b_{ap} at 530 nm (ω_{PA532} and ω_{PS530}, respectively), and PSAPCorr. There do not appear to be any obvious relationships between ambient or sample air RH and PA or PSAP optical properties. This is probably due to the generally dry conditions during the study.

The ratio (y/x) between raw 7-AE and PSAP b_{ap} ranged from 1.20 (470 nm/467 mm) to 1.29 (520 nm/530 nm). The corresponding ratios and average errors (AE) for adjusted 7-AE and PSAP b_{ap} ranged from 0.93 to 1.07 and −7 and 7%,

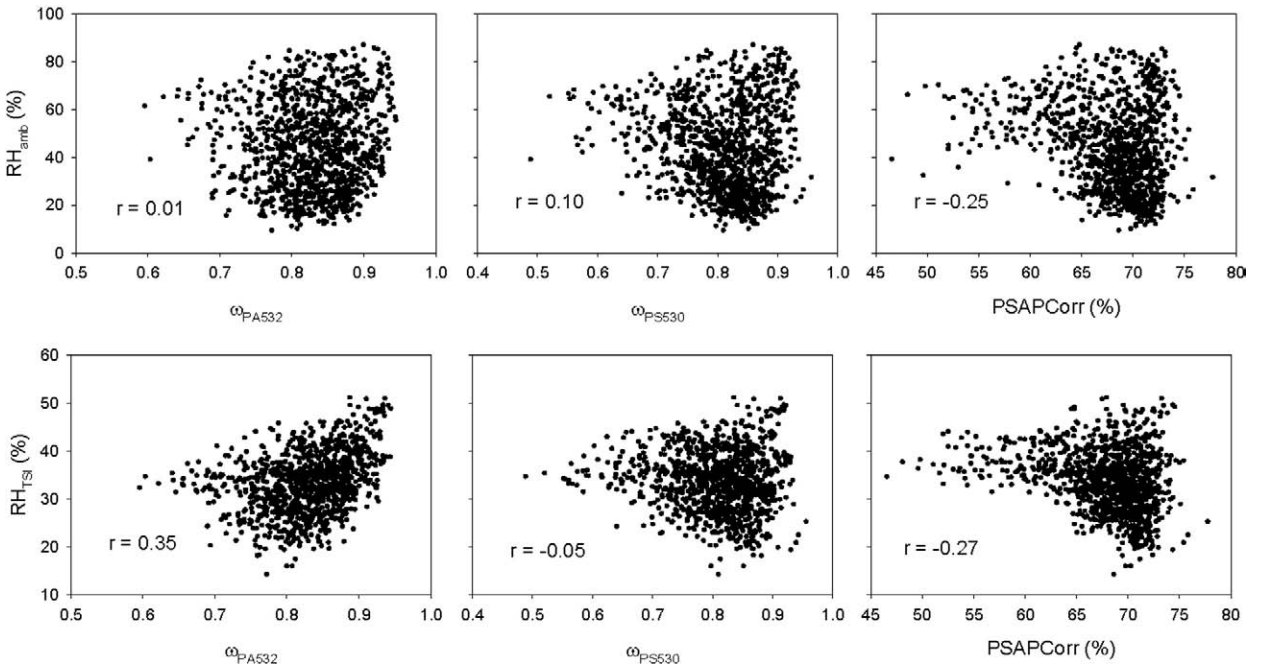

Fig. 1. Relationships among hourly average ambient relative humidity (RH_{amb}), RH in the TSI three wavelength nephelometer (RH_{TSI}), single-scattering albedo based on PA b_{ap} at 532 nm and PSAP b_{ap} at 530 nm (ω_{PA532} and ω_{PS530}, respectively), and the PSAP correction (PSAPCorr; the percent difference between raw and adjusted PSAP b_{ap} with respect to raw PSAP b_{ap}).

Table 5
Comparison statistics for 24-hour average black carbon (BC) and elemental carbon (EC) measurements at the Fresno Supersite, CA.

Instrument		Averages		OLS Regression[a]				r	N[c]	y/x		$y-x$			$(y-x)/x$	Distribution of $y-x$[g]			
Y	X	Y	x	Slope	SE[b]	Intercept	SE[b]			Average	SD[d]	Average	SD[d]	RMSE[e]	AE[f]	<1σe	1σ-2σ	2σ-3σ	>3σ
		(Mm^{-1})		(Mm^{-1})								(Mm^{-1})			(%)	(%)			
BC 7-AE 370 nm	BC 7-AE 950 nm	0.94	1.00	0.88	0.01	0.05	0.01	1.00	61	0.95	0.04	−0.06	0.06	0.19	−5	100.0	0.0	0.0	0.0
BC 7-AE 470 nm	BC 7-AE 950 nm	0.97	1.00	0.94	0.01	0.03	0.01	1.00	61	0.97	0.02	−0.03	0.03	0.19	−3	100.0	0.0	0.0	0.0
BC 7-AE 520 nm	BC 7-AE 950 nm	1.00	1.00	0.97	0.01	0.02	0.01	1.00	61	1.00	0.02	0.00	0.02	0.19	0	100.0	0.0	0.0	0.0
BC 7-AE 590 nm	BC 7-AE 950 nm	0.98	1.00	0.96	0.00	0.01	0.00	1.00	61	0.98	0.01	−0.03	0.02	0.19	−2	100.0	0.0	0.0	0.0
BC 7-AE 660 nm	BC 7-AE 950 nm	1.02	1.00	1.01	0.00	0.01	0.00	1.00	61	1.02	0.01	0.02	0.01	0.20	2	100.0	0.0	0.0	0.0
BC 7-AE 880 nm	BC 7-AE 950 nm	1.01	1.00	1.01	0.00	0.00	0.00	1.00	61	1.01	0.00	0.01	0.00	0.19	1	100.0	0.0	0.0	0.0
BC MAAP 670 nm	BC 7-AE 660 nm	1.08	1.08	1.00	0.02	0.00	0.03	0.99	39	0.99	0.06	0.00	0.06	0.26	−1	100.0	0.0	0.0	0.0
Sunset Optical BC	BC 7-AE 660 nm	0.53	0.97	0.59	0.03	−0.05	0.03	0.94	52	0.53	0.08	−0.44	0.16	0.25	−47	9.6	55.8	34.6	0.0
Sunset Optical BC	BC MAAP 670 nm	0.52	0.99	0.59	0.02	−0.06	0.02	0.99	30	0.51	0.05	−0.47	0.18	0.30	−49	16.7	63.3	20.0	0.0
IMPROVE_A_TOT EC	IMPROVE_A_TOR EC	0.76	1.01	0.71	0.04	0.05	0.04	0.95	49	0.77	0.09	−0.24	0.15	0.41	−23	91.8	8.2	0.0	0.0
STN_TOT EC	STN_TOR EC	0.57	0.82	0.58	0.07	0.09	0.06	0.90	18	0.71	0.12	−0.26	0.17	0.31	−29	77.8	16.7	5.6	0.0
STN_TOR EC	IMPROVE_A_TOR EC	0.82	0.98	0.71	0.07	0.12	0.07	0.94	18	0.91	0.28	−0.16	0.18	0.38	−10	100.0	0.0	0.0	0.0
French EC	IMPROVE_A_TOR EC	0.87	1.00	0.72	0.15	0.15	0.16	0.90	8	1.03	0.49	−0.13	0.23	0.34	3	75.0	25.0	0.0	0.0
Sunset Thermal EC	IMPROVE_A_TOR EC	0.58	1.01	0.62	0.05	−0.05	0.06	0.87	48	0.55	0.24	−0.44	0.21	0.43	−45	45.8	50.0	4.2	0.0
BC 7-AE 660 nm	IMPROVE_A_TOR EC	0.94	1.01	0.73	0.06	0.20	0.06	0.89	49	1.00	0.27	−0.07	0.19	0.37	0	87.8	12.2	0.0	0.0
BC MAAP 670 nm	IMPROVE_A_TOR EC	0.95	0.95	0.88	0.05	0.11	0.05	0.96	27	1.06	0.23	0.00	0.12	0.37	6	100.0	0.0	0.0	0.0
Sunset Optical BC	IMPROVE_A_TOR EC	0.52	1.01	0.47	0.04	0.04	0.04	0.87	48	0.53	0.13	−0.49	0.24	0.41	−47	27.1	72.9	0.0	0.0

[a]Ordinary least squares regression.
[b]Standard error.
[c]Number of data pairs.
[d]Standard deviation.
[e]Root mean squared errors (RMSE) = square root of sum of squares of the uncertainties for x and y.
[f]AE = Average error, 100 (average of $(y-x)/x$).
[g]Measurement difference of $(y-x)$ and distribution of measurement differences.

respectively. The differences between adjusted 7-AE and PSAP b_{ap} were less than twice their uncertainties in 90% of the cases over the three corresponding wavelengths. Thus, the correction algorithms for the 7-AE and PSAP resulted in similar b_{ap} measurements. Raw and adjusted 7-AE b_{ap} (660 nm) were 252% higher and 10% lower, respectively, than MAAP b_{ap} (670 nm). Raw and adjusted PSAP b_{ap} (660 nm) were 168% higher and 19% lower, respectively, than MAAP b_{ap} (670 nm).

The PA b_{ap} is considered the benchmark for this study. While raw 7-AE b_{ap} (520 nm) was 368% higher than PA b_{ap} (532 nm), adjusted 7-AE b_{ap} was only 24% higher. At higher λ, raw 7-AE b_{ap} (950 nm) was 616% higher than PA b_{ap} (1047 nm), but adjusted 7-AE b_{ap} was 69% higher. Table 4 also shows that when both 7-AE and PA b_{ap} were adjusted to 670 nm, 7-AE b_{ap} was 30% higher than PA b_{ap}. This demonstrates that Arnott et al.'s (2005) correction algorithm accounted for a large part of b_{ap} enhancement artifacts in the Aethalometer. However, under-adjustment was larger with increasing wavelength. This suggests that the wavelength dependence of the Aethalometer adjustment from kerosene soot aerosols (Arnott et al., 2005) may differ from that for ambient aerosols in Fresno.

All of the proposed adjustments for AE, PSAP, and MAAP b_{ap} overestimated b_{ap} measured with the PA for Fresno aerosols. The MAAP b_{ap} was 51% higher than PA b_{ap} at 670 nm. Adjusted PSAP b_{ap} at 530 nm was 17% higher than PA b_{ap} at 532 nm. Adjusted PSAP b_{ap} was 28% higher than PA b_{ap} at 670 nm. The relative magnitudes of the adjustment factors [b_{ap} (raw)/b_{ap} (adj)] were similar: i.e., 4.1 and 4.4 for the 7-AE at 590 and 880 nm, respectively, and 3.2 and 3.3 for the PSAP at 530 and 660 nm, respectively.

3.2. Comparison of BC and EC concentration

BC concentration is output directly by the Aethalometer, MAAP, and Sunset instruments, as described above. Table 5 compares 24-hour average BC measured by continuous optical instruments and EC measured with the IMPROVE_A, STN, French two-step, and Sunset carbon protocols. As 7-AE BC at 370, 470, 520, 590, 660, and 880 nm are compared to BC at 950 nm, all BC concentrations were within 5% according to the average error and average y/x. While the average concentrations were slightly lower at 370 and 470 nm, the differences were well within their measurement uncertainties.

7-AE (660 nm) and MAAP (670 nm) BC agreed to within 1%, similar to the 3% reported by Park et al. (2006) during summer 2004. However, the difference was much higher (10–20%) during winter of 2003–2004 (Park et al., 2006). All pair-wise correlations for the optical BC measurements were ≥0.94.

EC by TOR was 23% higher than EC by TOT following the IMPROVE_A protocol (Chow et al., 2007a) and 29% higher following the STN protocol (Peterson and Richards, 2002). As shown by Chow et al. (2004), these differences are smaller when TOR is used to determine the OC/EC split. STN_TOR was 10% lower than IMPROVE_A_TOR. EC by the French protocol was 3% higher than IMPROVE_A_TOR, although there were only eight data pairs in the comparison. EC by Sunset_TOT was 45% lower than IMPROVE_A_TOR. In all of these cases, the pair-wise correlations (r) were ≥0.87, and >94% of the paired differences were within twice their uncertainties.

Table 5 compares optical measures of BC with EC by IMPROVE_A_TOR. The average differences between 7-AE and MAAP BC versus IMPROVE_A_TOR EC were 0 and 6%, respectively. Sunset optical (660 nm) BC was 47% lower than IMPROVE_A_TOR. In all of these comparisons, correlations were ≥0.87 and 100% of the paired differences were within twice their uncertainties.

3.3. EC mass absorption efficiency (σ_{ap})

Table 6 presents average efficiencies calculated from 24-hour average PA b_{ap} at 532, 670, and 1047 nm and EC by IMPROVE_A, STN, French, and Sunset protocols. Because 29% of the hourly Sunset thermal EC concentrations were lower than their uncertainties, only 24-hour average Sunset EC concentrations larger than these uncertainties were used to estimate σ_{ap}.

Similar to b_{ap}, Table 6 shows σ_{ap} decreased with increasing wavelength for all thermal protocols. σ_{ap} at 532 nm ranged from 6.1 m^2/g for IMPROVE_A_TOR to 10.1 m^2/g for the STN_TOT protocol. The average σ_{ap} at 532 nm was 7.9 ± 1.5 m^2/g. The variation between protocols (19%) was less than the average variation within protocols (28%). This pattern was the same at 670 and 1047 nm, where the average efficiencies were 5.4 ± 1.1 and 2.8 ± 0.6 m^2/g, respectively. These values are within previously reported ranges of 2–25 m^2/g (e.g., Watson et al., 2005; Andreae and Gelencser, 2006; Bond and Bergstrom, 2006).

As mentioned above, factors that influence EC (or BC) absorption efficiency (e.g., particle size, density, refractive

Table 6
Mass absorption efficiencies (σ_{ap}, m^2/g) as the ratio of 24-hour average PA b_{ap} to EC concentrations by different methods at the Fresno Supersite.

Instrument		r	N[a]	σ_{ap} (y/x)		CV[c]
Y	X			Average	SD[b]	
b_{ap} (Mm^{-1})	EC ($\mu g/m^3$)					
PA 532 nm	IMPROVE_A_TOR EC	0.87	44	6.1	2.5	
PA 532 nm	IMPROVE_A_TOT EC	0.86	44	7.9	3.4	
PA 532 nm	STN_TOR EC	0.89	17	7.0	1.1	
PA 532 nm	STN_TOT EC	0.89	17	10.1	2.1	
PA 532 nm	French EC	0.93	7	7.0	1.3	
PA 532 nm	Sunset Thermal EC[d]	0.88	38	9.3	2.4	
Average				7.9	1.5	(19%)
PA 670 nm[e]	IMPROVE_A_TOR EC	0.87	41	4.2	1.7	
PA 670 nm[e]	IMPROVE_A_TOT EC	0.86	41	5.5	2.3	
PA 670 nm[e]	STN_TOR EC	0.87	15	4.8	0.8	
PA 670 nm[e]	STN_TOT EC	0.87	15	7.0	1.5	
PA 670 nm[e]	French EC	0.98	5	4.6	0.6	
PA 670 nm[e]	Sunset Thermal EC[d]	0.87	35	6.5	1.7	
Average				5.4	1.1	(20%)
PA 1047 nm	IMPROVE_A_TOR EC	0.87	45	2.1	0.8	
PA 1047 nm	IMPROVE_A_TOT EC	0.83	45	2.8	1.1	
PA 1047 nm	STN_TOR EC	0.88	16	2.5	0.4	
PA 1047 nm	STN_TOT EC	0.90	16	3.6	0.6	
PA 1047 nm	French EC	0.98	6	2.3	0.3	
PA 1047 nm	Sunset Thermal EC[d]	0.91	39	3.4	0.7	
Average				2.8	0.6	(21%)

[a] Number of data pairs.
[b] Standard deviation.
[c] Coefficient of variation.
[d] Only 24-h average Sunset thermal EC concentrations larger than their uncertainties were used.
[e] b_{ap} scaled to 670 nm based on log–log interpolation between 532 and 1047 nm.

index, and morphology; Bond, 2001) are not well characterized and a single σ_{ap} cannot provide optical closure in all environments, or even at different times in the same environment. The Fresno efficiencies should be considered upper limits because OC may also contribute to b_{ap}, especially at $\lambda < 532$ nm. The calculated Fresno absorption efficiencies of 6.1 and 2.1 m^2/g at 532 and 1047 nm, respectively, are 20% and 60% lower than the corresponding PA defaults (7.5 and 5.0 m^2/g, respectively) determined from kerosene soot (Sheridan et al., 2005) and diesel vehicle emissions (Arnott et al., 2005). Differences in optical properties are related to physical differences in the absorbing material, which, in turn, may lead to differences in the OC/EC split.

3.4. Derivation of the absorption Angström exponent (α)

Fig. 2 presents average b_{ap} as a function of λ for different b_{ap}/BC instruments. As seen in Table 4, b_{ap} consistently decreased with increasing λ. The spectral dependence of aerosol light absorption is described by Eqs. (1) and (3). The theoretical value of α in Eq. (3) is equal to unity for small spherical absorbing particles, while values between 0.94 and 1.0 were measured for kerosene soot (Bond, 2001; Sheridan et al., 2005). However, the absorption of light at small wavelengths by non-graphitic compounds will change the relationship between b_{ap} and λ (Kirchstetter et al., 2004; Andreae and Gelencser, 2006; Chen et al., 2006). Averages and standard deviations of 24-hour average α for raw and adjusted b_{ap} are presented in Table 7. Without adjustment, the α value based on raw b_{ap} ranged from 0.92 ± 0.04 for the 2-AE to 1.02 ± 0.04 for the PSAP. Estimates of α based on adjusted b_{ap} ranged 1.19 ± 0.10 for the 7-AE to 1.46 ± 0.25 for the PA. The slope ($-\alpha$) in Eq. (3) was less steep for adjusted b_{ap} because the multiple scattering correction is reduced as a function of the total aerosol absorption optical depth on the filter, which increases with decreasing λ.

Table 7
Average Angström exponents (α) from 24-hour average b_{ap} measurements at multiple wavelengths.

Instrument	Angström exponent (α)	Number of samples
2-AE (raw)	0.92 ± 0.04[a]	61
7-AE (raw)	0.94 ± 0.04	61
PSAP(raw)	1.02 ± 0.04	44
2-AE (adjusted)	1.23 ± 0.10	53
7-AE (adjusted)	1.19 ± 0.10	53
PSAP (adjusted)	1.28 ± 0.06	44
PA	1.46 ± 0.25	43

[a]Average $\pm$ standard deviation.

3.5. Diurnal variations and implications for sources

Fig. 3 presents the hourly average diurnal variation of BC ($\mu g/m^3$) derived from PA b_{ap} at 532 nm using a value of 7.9 m^2/g for σ_{ap} (Table 6), OC ($\mu g/m^3$) measured with the Sunset thermal protocol, the ratio of BC/TC, where TC = OC + BC, the ratio of OC/TC, and α derived from PA and 7-AE b_{ap}. The BC from PA was chosen for this analysis because a large number of the Sunset thermal EC concentrations were below MDL. BC concentration peaked at 0600 Pacific Daylight Time (PDT; GMT-8), coinciding with the morning rush hour. As the day progressed, BC decreased as the mixed layer deepened and reached a minimum between 1500 and 1700 PDT. BC peaked again at 1900 PDT during the evening rush hour and remained elevated through the night in the shallow inversion layer (Watson and Chow, 2002b). OC peaked later than BC, between 0800 and 1300 PDT, suggesting that OC originated from sources other than motor vehicles, such as cooking or SOA (Magliano et al., 1999; Chow et al., 2006c; Chen et al., 2007).

The BC/TC ratio exhibited the same diurnal variation as BC. However, the OC/TC ratio increased throughout the day, as BC decreased, and peaked between 1500 and 1700 PDT (Watson et al., 2006). This could reflect photochemical production of SOA during the afternoon hours, which also lowered the BC/TC ratio. The diurnal variation of α derived from both PA and 7-AE b_{ap}, was similar to that of the OC/TC ratio. This suggests that the afternoon increase in α was caused by additional light absorption by SOA. The lowest values of α occurred during the morning rush hours. Kirchstetter et al. (2004) suggested that a value of α close

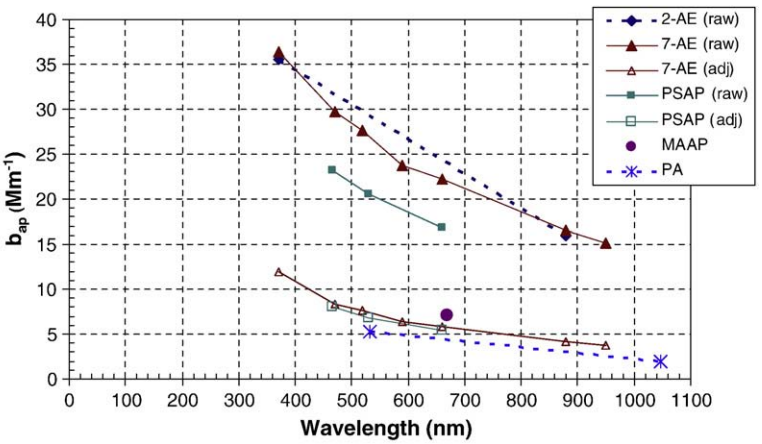

Fig. 2. Average particle light absorption (b_{ap}) measured with different instruments as a function of wavelength (2-AE: dual-wavelength aethalometer at 370 and 880 nm; 7-AE: seven-color aethalometer at 370, 470, 520, 590, 660, 880, and 950 nm; PSAP: three wavelength particle soot absorption photometer at 467, 530 and 660 nm; MAAP: Multi-angle absorption photometer at 670 nm; and PA: two photoacoustic instruments at 532 and 1047 nm, respectively).

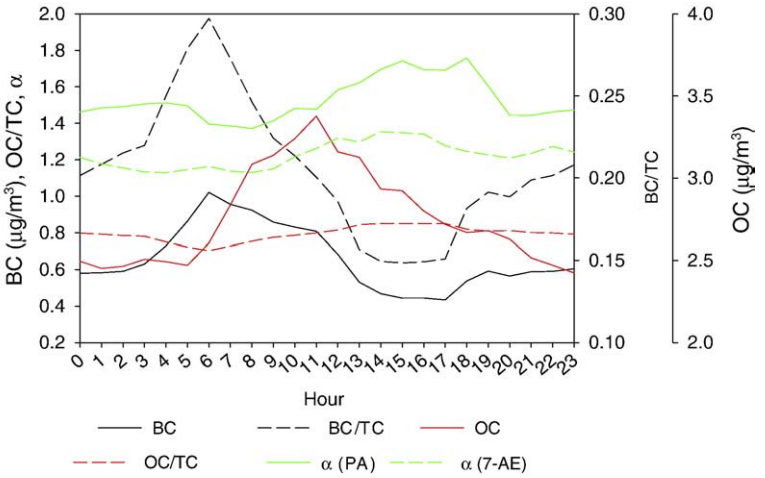

Fig. 3. Average diurnal variation of BC (PA 532 nm), OC (Sunset thermal), BC/TC (TC = OC + BC), OC/TC, and Angström absorption exponent (α) derived from PA and adjusted 7-AE b_{ap}. Hour is Pacific Daylight Time (PDT; GMT − 8).

to unity indicates weak spectral dependence of b_{ap} commonly associated with fresh diesel soot. Values higher than unity throughout the day in Fresno suggest that organic aerosol also contributed to particle light absorption.

4. Conclusions

Aerosol light absorption (b_{ap}) by two- and seven-wavelength Aethalometers (2- and 7-AE), a three wavelength Particle Soot Absorption Photometer (PSAP), a Multi-Angle Absorption Photometer (MAAP), and two Photoacoustic Analyzers (PA); black carbon (BC); and elemental carbon (EC) measurements were compared at the Fresno Supersite during summer 2005. The PA measured in-situ b_{ap} and was used as a reference. On average, uncorrected (raw) AE and PSAP b_{ap} were 4.7–7.2 and 3.7–4.1 times higher, respectively, than corresponding PA b_{ap}. These large differences were due to artifactual enhancement of b_{ap} by filter loading, back-scattering, and multiple scattering by particles and the filter matrix. After applying published algorithms to correct for these effects, the adjusted AE b_{ap} was 24–69% higher and PSAP b_{ap} was 17–28% higher than PA b_{ap} with greater differences at higher wavelengths. The MAAP, which implicitly corrects for these effects by design, measured 51% higher b_{ap} than the PA. Published algorithms for correcting Aethalometer and PSAP b_{ap} produced very similar results.

The AE and MAAP convert raw b_{ap} to BC (μg/m^3) with default factors of $14625/\lambda$ and 6.6 m^2/g, respectively. The Sunset instrument estimates BC with an empirical function of light transmission and EC measured with its thermal analysis. On average, agreement between AE (660 nm) and MAAP (670 nm) BC was within 1%. BC determined with the Sunset instrument was 47% and 49% lower than BC measured with the AE and MAAP, respectively. EC was measured on 24-hour integrated filter samples with IMPROVE_A, STN, French, and Sunset protocols. On average, TOT EC was 23% and 29% lower than TOR EC for the IMPROVE_A and STN protocols, respectively. Within TOR protocols, EC from IMPROVE_A was 10% higher than STN, within 3% of French two-step, and 45% higher than Sunset TOT EC.

Mass absorption efficiencies (σ_{ap}, m^2/g) were estimated from b_{ap} measured with the PA and EC measured with various protocols. σ_{ap} averaged 7.9 ± 1.5, 5.4 ± 1.1, and 2.8 ± 0.6 m^2/g over all EC analysis protocols at wavelengths of 532, 670, and 1047 nm, respectively. The average σ_{ap} at 532 nm is similar to values found in the literature (7.5 ± 1.2 m^2/g at 550 nm) for uncoated (fresh) EC particles. The Angström exponent (α) describes the wavelength dependence of b_{ap}. On average, α ranged from 1.2 to 1.46 based on adjusted b_{ap} measured with the 7-AE and the PA, respectively. The largest α values occurred during the afternoon hours when the organic fraction of total carbon was highest. This increase may be related to photochemical production of secondary organic aerosols that preferentially absorb light at low wavelengths. While most of these measurements were well correlated, biases in filter-based light absorption and thermal carbon measurements must be identified and corrected for accurate determination of b_{ap}, BC, and EC in different environments.

Acknowledgements

This research was co-sponsored by the California Air Resources Board (CARB) and the United States' Environmental Protection Agency (EPA) Supersites program. The conclusions are those of the authors and do not necessarily reflect the views of the sponsoring agencies. Any mention of commercially available products and supplies does not constitute an endorsement of those products and supplies. The authors thank Scott Scheller of CARB for maintaining the monitoring instruments; Steve Kohl and Dana Trimble for their assistance with data validation, and Jo Gerrard for editing the manuscript.

References

Ackerman, A.S., Toon, O.B., Stevens, D.E., Heymsfield, A.J., Ramanathan, V., Welton, E.J., 2000. Reduction of tropical cloudiness by soot. Science 288, 1042–1047.

Anderson, T.L., Ogren, J.A., 1998. Determining aerosol radiative properties using the TSI 3563 integrating nephelometer. Aerosol Sci. Technol. 29, 57–69.

Andreae, M.O., Gelencser, A., 2006. Black carbon or brown carbon? The nature of light-absorbing carbonaceous aerosols. Atmos. Chem. Phys. 6, 3131–3148.
Arnott, W.P., Moosmüller, H., Rogers, C.F., Jin, T., Bruch, R., 1999. Photoacoustic spectrometer for measuring light absorption by aerosol: instrument description. Atmos. Environ. 33, 2845–2852.
Arnott, W.P., Moosmüller, H., Walker, J.W., 2000. Nitrogen dioxide and kerosene-flame soot calibration of photoacoustic instruments for measurement of light absorption by aerosols. Rev. Sci. Instrum. 71, 4545–4552.
Arnott, W.P., Moosmüller, H., Sheridan, P.J., Ogren, J.A., Raspet, R., Slaton, W.V., Hand, J.L., Kreidenweis, S.M., Collett Jr., J.L., 2003. Photoacoustic and filter-based ambient aerosol light absorption measurements: instrument comparison and the role of relative humidity. J. Geophys. Res. 108. doi:10.1029/2002JD002165 AAC 15-1–AAC 15-11.
Arnott, W.P., Hamasha, K., Moosmüller, H., Sheridan, P.J., Ogren, J.A., 2005. Towards aerosol light-absorption measurements with a 7-wavelength aethalometer: evaluation with a photoacoustic instrument and 3-wavelength nephelometer. Aerosol Sci. Technol. 39, 17–29.
Bae, M.S., Schauer, J.J., Deminter, J.T., Turner, J.R., Smith, D., Cary, R.A., 2004. Validation of a semi-continuous instrument for elemental carbon and organic carbon using a thermal-optical method. Atmos. Environ. 38, 2885–2893.
Bell, A.G., 1881. Production of sound by radiant energy. Manuf. Build. 15, 156–158 http://cdl.library.cornell.edu/cgi-bin/moa/moa-cgi?notisid = ABS1821-0013-416.
Bevington, P.R., 1969. Data Reduction and Error Analysis for the Physical Sciences. McGraw Hill, New York, NY.
Birch, M.E., 1998. Analysis of carbonaceous aerosols: interlaboratory comparison. Analyst 123, 851–857.
Birch, M.E., Cary, R.A., 1996a. Elemental carbon-based method for monitoring occupational exposures to particulate diesel exhaust. Aerosol Sci. Technol. 25, 221–241.
Birch, M.E., Cary, R.A., 1996b. Elemental carbon-based method for occupational monitoring of particulate diesel exhaust: methodology and exposure issues. Analyst 121, 1183–1190.
Bond, T.C., Anderson, T.L., Campbell, D.E., 1999. Calibration and intercomparison of filter-based measurements of visible light absorption by aerosols. Aerosol Sci.Technol. 30, 582–600.
Bond, T.C., 2001. Spectral dependence of visible light absorption by carbonaceous particles emitted from coal combustion. Geophys. Res. Lett. 28, 4075–4078.
Bond, T.C., Bergstrom, R.W., 2006. Light absorption by carbonaceous particles: an investigative review. Aerosol Sci. Technol. 40, 27–67.
Cachier, H., Bremond, M.P., Buat-Ménard, P., 1989a. Determination of atmospheric soot carbon with a simple thermal method. Tellus 41B, 379–390.
Cachier, H., Bremond, M.P., Buat-Ménard, P., 1989b. Thermal separation of soot carbon. Aerosol Sci. Technol. 10, 358–364.
Chen, L.-W.A., Moosmüller, H., Arnott, W.P., Chow, J.C., Watson, J.G., Susott, R.A., Babbitt, R.E., Wold, C., Lincoln, E., Hao, W.M., 2006. Particle emissions from laboratory combustion of wildland fuels: in situ optical and mass measurements. Geophys. Res. Lett. 33, 1–4. doi:10.1029/2005GL024838.
Chen, L.-W.A., Watson, J.G., Chow, J.C., Magliano, K.L., 2007. Quantifying $PM_{2.5}$ source contributions for the San Joaquin valley with multivariate receptor models. Environ. Sci. Technol. 41, 2818–2826.
Chow, J.C., Watson, J.G., Pritchett, L.C., Pierson, W.R., Frazier, C.A., Purcell, R.G., 1993. The DRI thermal/optical reflectance carbon analysis system: description, evaluation and applications in U.S. air quality studies. Atmos. Environ. 27A, 1185–1201.
Chow, J.C., Watson, J.G., Crow, D., Lowenthal, D.H., Merrifield, T.M., 2001. Comparison of IMPROVE and NIOSH carbon measurements. Aerosol Sci. Technol. 34, 23–34.
Chow, J.C., Bachmann, J.D., Wierman, S.S.G., Mathai, C.V., Malm, W.C., White, W.H., Mueller, P.K., Kumar, N.K., Watson, J.G., 2002. 2002 Critical review discussion — visibility: science and regulation. J. Air Waste Manage. Assoc. 52, 973–999.
Chow, J.C., Watson, J.G., Chen, L.-W.A., Arnott, W.P., Moosmüller, H., Fung, K.K., 2004. Equivalence of elemental carbon by thermal/optical reflectance and transmittance with different temperature protocols. Environ. Sci. Technol. 38, 4414–4422.
Chow, J.C., Watson, J.G., Chen, L.-W.A., Paredes-Miranda, G., Chang, M.-C.O., Trimble, D., Fung, K.K., Zhang, H., Yu, J.Z., 2005a. Refining temperature measures in thermal/optical carbon analysis. Atmos. Chem. Phys. 5 (4), 2961–2972.
Chow, J.C., Watson, J.G., Louie, P.K.K., Chen, L.-W.A., Sin, D., 2005b. Comparison of $PM_{2.5}$ carbon measurement methods in Hong Kong, China. Environ. Poll. 137, 334–344.
Chow, J.C., Watson, J.G., Mauderly, J.L., Costa, D.L., Wyzga, R.E., Vedal, S., Hidy, G.M., Altshuler, S.L., Marrack, D., Heuss, J.M., Wolff, G.T., Pope III, C.A., Dockery, D.W., 2006a. 2006 Critical review discussion — health effects of fine particulate air pollution: lines that connect. J. Air Waste Manage. Assoc. 56, 1368–1380.
Chow, J.C., Watson, J.G., Doraiswamy, P., Chen, L.-W.A., Sodeman, D.A., Ho, S.S.H., Kohl, S.D., Trimble, D.L., Voepel, H., Fung, K.K., 2006b. Climate change — characterization of Black Carbon and Organic Carbon Air Pollution Emissions and Evaluation of Measurement Methods. Phase I: method intercomparison. Desert Research Institute, Reno, NV, for California Air Resources Board, Sacramento, CA. http://www.arb.ca.gov/research/apr/past/04-307_v2.pdf.
Chow, J.C., Chen, L.-W.A., Watson, J.G., Lowenthal, D.H., Magliano, K.L., Turkiewicz, K., Lehrman, D., 2006c. $PM_{2.5}$ chemical composition and spatiotemporal variability during the California regional $PM_{10}/PM_{2.5}$ Air Quality Study (CRPAQS). J. Geophys. Res.-Atmospheres 111, 1–17. doi:10.1029/2005JD006457.
Chow, J.C., Watson, J.G., Chen, L.W.A., Chang, M.C.O., Robinson, N.F., Trimble, D., Kohl, S., 2007a. The IMPROVE_A temperature protocol for thermal/optical carbon analysis: maintaining consistency with a long-term database. J. Air Waste Manage. Assoc. 57, 1014–1023.
Chow, J.C., Watson, J.G., Lowenthal, D.H., Chen, L.-W.A., Zielinska, B., Mazzoleni, L.R., Magliano, K.L., 2007b. Evaluation of organic markers for chemical mass balance source apportionment at the Fresno Supersite. Atmos. Chem. Phys. 7, 1741–2754.
Chow, J.C., Doraiswamy, P., Watson, J.G., Chen, L.-W.A., Ho, S.S.H., Sodeman, D.A., 2008. Advances in integrated and continuous measurements for particle mass and chemical composition. J. Air Waste Manage. Assoc. 58, 141–163.
Chow, J.C., Watson, J.G., Lowenthal, D.H., Chen, L.-W.A., 2009. Climate change — characterization of black carbon and organic carbon air pollution emissions and evaluation of measurement methods. Prepared by Desert Research Institute, Reno, NV, for the California Air Resources Board, Sacramento, CA. http://www.arb.ca.gov/research/apr/past/04-307_v2.pdf.
Currie, L.A., Benner Jr., B.A., Cachier, H., Cary, R., Chow, J.C., Druffel, E.R.M., Eglinton, T.I., Gustafsson, Ö., Hartmann, P.C., Hedges, J.I., Kessler, J.D., Kirchstetter, T.W., Klinedinst, D.B., Klouda, G.A., Marolf, J.V., Masiello, C.A., Novakov, T., Pearson, A., Prentice, K.M., Puxbaum, H., Quinn, J.G., Reddy, C.M., Schmid, H., Slater, J.F., Watson, J.G., Wise, S.A., 2002. A critical evaluation of interlaboratory data on total, elemental, and isotopic carbon in the carbonaceous particle reference material, NIST SRM 1649a. J. Res. National Bureau Standards 107, 279–298.
Gundel, L.A., Dod, R.L., Rosen, H., Novakov, T., 1984. The relationship between optical attenuation and black carbon concentration for ambient and source particles. Sci.Total Environ. 36, 197–202.
Hansen, A.D.A., Rosen, H., Novakov, T., 1984. The aethalometer — an instrument for the real-time measurement of optical absorption by aerosol particles. Sci. Total Environ. 36, 191–196.
Hansen, A.H.A., 2005. The Aethalometer. Magee Scientific Company, Berkeley, CA.
Horvath, H., 1993. Atmospheric light absorption — a review. Atmos. Environ. 27A, 293–317.
Jacobson, M.Z., 2001. Strong radiative heating due to the mixing state of black carbon in atmospheric aerosols. Nature 409, 695–697.
Japar, S.M., Moore, J., Killinger, D.K., Szkarlat, A.C., 1982. Spectrophone measurements of diesel vehicle particulate material. In: Gerber, H.E., Hindman, E.E. (Eds.), Light Absorption by Aerosol Particles. Spectrum Press, Hampton, VA, pp. 275–278.
Kirchstetter, T.W., Novakov, T., Hobbs, P.V., 2004. Evidence that the spectral dependence of light absorption by aerosols is affected by organic carbon. J. Geophys. Res.-Atmospheres 109, D21208. doi:10.1029/2004JD004999.
Magliano, K.L., Hughes, V.M., Chinkin, L.R., Coe, D.L., Haste, T.L., Kumar, N.K., Lurmann, F.W., 1999. Spatial and temporal variations in PM_{10} and $PM_{2.5}$ source contributions and comparison to emissions during the 1995 integrated monitoring study. Atmos. Environ. 33, 4757–4773.
Mauderly, J.L., Chow, J.C., 2008. Health effects of organic aerosols. Inhal. Toxicol. 20, 257–288. doi:10.1080/08958370701866008.
McCracken, M.C., 2008. Critical review: prospects for future climate change and the reasons for early action. J. Air Waste Manage. Assoc. 58, 735–786. doi:10.3155/1047-3289.58.6.735.
Murphy, D.M., 2009. The effect of water evaporation on photoacoustic signals in transition and molecular flow. Aerosol Sci. Technol. 43, 356–363.
Park, K., Chow, J.C., Watson, J.G., Trimble, D.L., Doraiswamy, P., Arnott, W.P., Stroud, K.R., Bowers, K., Bode, R., Petzold, A., Hansen, A.D.A., 2006. Comparison of continuous and filter-based carbon measurements at the Fresno Supersite. J. Air Waste Manage. Assoc. 56, 474–491.
Peterson, M.R., Richards, M.H., 2002. Thermal–optical–transmittance analysis for organic, elemental, carbonate, total carbon, and OCX2 in $PM_{2.5}$ by the EPA/NIOSH method. In: Winegar, E.D., Tropp, R.J. (Eds.), Proceedings, Symposium on Air Quality Measurement Methods and Technology-2002. InAir & Waste Management Association, Pittsburgh, PA, pp. 83–1-83-19.

Petzold, A., Schönlinner, M., 2004. Multi-angle absorption photometry — a new method for the measurement of aerosol light absorption and atmospheric black carbon. J. Aerosol Sci. 35, 421–441.
Petzold, A., Kramer, H., Schönlinner, M., 2002. Continuous measurement of atmospheric black carbon using a multi-angle absorption photometer. Environ. Sci. Pollut. Res. 78–82.
Petzold, A., Schloesser, H., Sheridan, P.J., Arnott, W.P., Ogren, J.A., Virkkula, A., 2005. Evaluation of multiangle absorption photometry for measuring aerosol light absorption. Aerosol Sci. Technol. 39, 40–51.
Pope III, C.A., Dockery, D.W., 2006. Critical review: health effects of fine particulate air pollution: lines that connect. J. Air Waste Manage. Assoc. 56, 709–742.
Roessler, D.M., 1984. Photoacoustic insights on diesel exhaust particles. Appl. Opt. 23, 1148–1155.
Schauer, J.J., Cass, G.R., 2000. Source apportionment of wintertime gas-phase and particle-phase air pollutants using organic compounds as tracers. Environ. Sci. Technol. 34, 1821–1832.
Schmid, H.P., Laskus, L., Abraham, H.J., Baltensperger, U., Lavanchy, V.M.H., Bizjak, M., Burba, P., Cachier, H., Crow, D., Chow, J.C., Gnauk, T., Even, A., ten Brink, H.M., Giesen, K.P., Hitzenberger, R., Hueglin, C., Maenhaut, W., Pio, C.A., Puttock, J., Putaud, J.P., Toom-Sauntry, D., Puxbaum, H., 2001. Results of the "Carbon Conference" international aerosol carbon round robin test: stage 1. Atmos. Environ. 35, 2111–2121.
Schmidt, M.W.I., Skjemstad, J.O., Czimczik, C.I., Glaser, B., Prentice, K.M., Gelinas, Y., Kuhlbusch, T.K., 2001. Comparative analysis of black carbon in soils. Glob. Biogeochem. Cycles 15, 163–167.
Sheridan, P.J., Arnott, W.P., Ogren, J.A., Andrews, E., Atkinson, D.B., Covert, D.S., Moosmüller, H., Petzold, A., Schmid, B., Strawa, A.W., Varma, R., Virkkula, A., 2005. The Reno aerosol optics study: an evaluation of aerosol absorption measurement methods. Aerosol Sci. Technol. 39, 1–16.
Virkkula, A., Ahlquist, N.C., Covert, D.S., Arnott, W.P., Sheridan, P.J., Quinn, P.K., Coffman, D.J., 2005. Modification, calibration and a field test of an instrument for measuring light absorption by particles. Aerosol Sci. Technol. 39, 68–83.
Watson, J.G., 2002. Visibility: science and regulation. J. Air Waste Manage. Assoc. 52, 628–713.
Watson, J.G., Chow, J.C., 2002a. Comparison and evaluation of in-situ and filter carbon measurements at the Fresno Supersite. J. Geophys. Res. 107. doi:10.1029/2001JD000573 ICC 3-1–ICC 3-15.
Watson, J.G., Chow, J.C., 2002b. A wintertime $PM_{2.5}$ episode at the Fresno, CA, Supersite. Atmos. Environ. 36, 465–475.
Watson, J.G., Chow, J.C., Bowen, J.L., Lowenthal, D.H., Hering, S., Ouchida, P., Oslund, W., 2000. Air quality measurements from the Fresno Supersite. J. Air Waste Manage. Assoc. 50, 1321–1334.
Watson, J.G., Turpin, B.J., Chow, J.C., 2001. The measurement process: precision, accuracy, and validity, In: Cohen, B.S., McCammon, C.S.J. (Eds.), Air Sampling Instruments for Evaluation of Atmospheric Contaminants, Ninth Edition. American Conference of Governmental Industrial Hygienists, Cincinnati, OH, pp. 201–216.
Watson, J.G., Chow, J.C., Chen, L.-W.A., 2004. Summary of methods and comparison studies for organic and elemental carbon: implications for visibility and global warming. In: Pitchford, M., Poirot, R. (Eds.), Proceedings, Regional and Global Perspectives on Haze: Causes, Consequences and Controversies Visibility Specialty Conference. Air and Waste Management Association, Pittsburgh, PA, pp. 55-1–55-38.
Watson, J.G., Chow, J.C., Chen, L.-W.A., 2005. Summary of organic and elemental carbon/black carbon analysis methods and intercomparisons. AAQR 5, 65–102. http://www.aaqr.org.
Watson, J.G., Chow, J.C., Park, K., Lowenthal, D.H., 2006. Nanoparticle and ultrafine particle events at the Fresno Supersite. J. Air Waste Manage. Assoc. 56, 417–430.
Watson, J.G., Chen, L.-W.A., Chow, J.C., Lowenthal, D.H., Doraiswamy, P., 2008. Source apportionment: findings from the U.S. Supersite Program. J. Air Waste Manage. Assoc. 58, 265–288.